

Probing the Initial Stage of Aggregation of the A β ₁₀₋₃₅-protein: Assessing the Propensity for Peptide Dimerization

Bogdan Tarus¹, John E. Straub^{1*} and D. Thirumalai^{2,3*}

¹Department of Chemistry
Boston University, Boston
MA 02215, USA

²Institute for Physical Science
and Technology, University of
Maryland, College Park, MD
20742, USA

³Department of Chemistry and
Biochemistry, University of
Maryland, College Park, MD
20742, USA

Characterization of the early stages of peptide aggregation is of fundamental importance in elucidating the mechanism of the formation of deposits associated with amyloid disease. The initial step in the pathway of aggregation of the A β -protein, whose monomeric NMR structure is known, was studied through the simulation of the structure and stability of the peptide dimer in aqueous solution. A protocol based on shape complementarity was used to generate an assortment of possible dimer structures. The structures generated based on shape complementarity were evaluated using rapidly computed estimates of the desolvation and electrostatic interaction energies to identify a putative stable dimer structure. The potential of mean force associated with the dimerization of the peptides in aqueous solution was computed for both the hydrophobic and the electrostatic driven forces using umbrella sampling and classical molecular dynamics simulation at constant temperature and pressure with explicit solvent and periodic boundary conditions. The comparison of the two free energy profiles suggests that the structure of the peptide dimer is determined by the favorable desolvation of the hydrophobic residues at the interface. Molecular dynamics trajectories originating from two putative dimer structures indicate that the peptide dimer is stabilized primarily through hydrophobic interactions, while the conformations of the peptide monomers undergo substantial structural reorganization in the dimerization process. The finding that the ϕ -dimer may constitute the ensemble of stable A β ₁₀₋₃₅ dimer has important implications for fibril formation. In particular, the expulsion of water molecules at the interface might be a key event, just as in the oligomerization of A β ₁₆₋₂₂ fragments. We conjecture that events prior to the nucleation process themselves might involve crossing free energy barriers which depend on the peptide–peptide and peptide–water interactions. Consistent with existing experimental studies, the peptides within the ensemble of aggregated states show no signs of formation of secondary structure.

© 2004 Elsevier Ltd. All rights reserved.

Keywords: Alzheimer's disease; amyloid β -protein; dimer; molecular dynamics simulation; potential of mean force

*Corresponding authors

Introduction

Amyloid β -protein (A β) is involved in the

Abbreviations used: A β , amyloid β -protein; AD, Alzheimer's disease; LMW, low molecular weight; PMF, potential of mean force; RMSD, root-mean-square displacement; CD, circular dichroism; ACE, atomic contact energy; DCOM, distance between centers-of-mass.

E-mail addresses of the corresponding authors:
straub@bu.edu; thirum@glue.umd.edu

pathogenesis of Alzheimer's disease (AD).^{1,2} Early studies illustrated the presence of amyloid plaques in the human brain of AD victims, and these conglomerates have been related to the evolution of AD.³ It is still not established whether amyloid protein aggregates, fibrils or plaques are causative agents of the pathological manifestations or whether they are only collateral products of this disease.³ However, the toxic influence of the amyloid plaques on the proximate neurons has been demonstrated.⁴⁻⁶ Recent studies have found that the neurotoxicity may be provoked even by

mobile low molecular weight (LMW) aggregates of A β .⁷⁻⁹ The oligomeric structures of A β are also involved in the early steps of fibrilization.¹⁰ Teplow and co-workers have analyzed the role of A β in the nucleation phase, showing that two alloforms, A β_{1-40} and A β_{1-42} , follow different pathways in the fibril formation process.¹¹ They hypothesized that the peptides initially form paranuclei and that those nuclei further form, through a linear aggregation mechanism, amyloidic fibrils.¹¹ These observations give rise to the question of how the structure of the monomer will influence the kinetics of fibril formation. Massi *et al.*¹² compared the conformational fluctuations of A β_{10-35} wild-type with the more amyloidogenic Dutch mutant of the same fragment using molecular dynamics simulation. They concluded that there is not much difference in the intrapeptide interactions corresponding to the two peptides and that the enhanced amyloidogenic propensity of the Dutch mutant results from its decreased hydrophilicity.¹² Recently, Bitan *et al.*¹³ analyzed the differences in oligomerization of two alloforms, A β_{1-40} and A β_{1-42} . It is known that the fibrilization kinetics of A β_{1-42} is faster than that of A β_{1-40} .^{14,15} They observed that the oxidation of Met35 in A β_{1-42} reduced the rate of fibril formation, rendering it comparable to that of A β_{1-40} . It was postulated that the increased hydrophilicity of the oxidized mutant will result in a larger free energy barrier to oligomerization.¹³ These studies all point to the essential role of intermonomeric interactions, in the formation of LMW aggregates, and the role of LMW aggregates as essential intermediates in the process of amyloidogenesis.¹⁶

Solid-state NMR studies of amyloid fibrils have revealed that A β adopts a parallel in-register organization in β -sheets for both A β_{10-35} ¹⁷ and A β_{1-40} .^{18,19} Those structures raise the question, by what mechanism does the native collapsed random coil structure of the monomeric A β undergo conformational transition to the β -strand conformation characteristic of the fibrils? Recent experimental and computational studies have led to the conjecture that a transient α -helical phase is a necessary on-pathway intermediate¹⁶ connecting the monomeric peptide with the β -strand conformations of the fibrils for A β_{1-40} ²⁰ and A β_{16-22} .²¹ These data suggest a central role for LMW aggregates in the A β aggregation pathway and possibly the evolution of AD itself. It may be that an efficient therapy for AD is to prevent the formation of LMW aggregation of A β .

In this work, we study the initial step in the oligomerization process of A β_{10-35} , which is the process of A β_{10-35} dimerization. The initial configuration of the system was obtained using a protein docking protocol. Two possible initial structures were obtained, and the best one was selected based on energetic considerations. Finally, the stability of the dimer and the secondary structure elements' fluctuations were analyzed *via* classical molecular dynamics.

The major reason for using the A β_{10-35} in this

study is that there is an aqueous solution NMR structure for this fragment of the protein. Knowledge of the starting structure for such a large peptide represents an important advantage in our *in silico* experiment. Guessing the structure of the A β_{1-42} , starting from A β_{10-35} will add uncertainty to our results. The lack of a 3D structure for the A β_{1-42} is not the only impediment for an atomic resolution dimerization study. The experimental observations report a high flexibility of the A β_{1-42} termini in aqueous solvent, and, consequently, it is very difficult to find an initial dimer structure. The flexible structure of the A β_{1-42} will also increase the size of the system studied (the protein and the explicit solvent) to such an extent that the simulations become prohibitive. We note that besides Maggio's studies^{22,23} of the A β_{10-35} structure and properties, Lynn showed that A β_{10-35} adopts a parallel in-register organization in β -sheets.¹⁷

Results and Discussion

Outline

As our study consists of a number of parts, and both atomistic and coarse-grained models are employed, an overview of the study is provided as an outline.

Generation of putative dimer structures

The generation of the two A β_{10-35} -protein dimer decoy sets was the first step of our study. A coarse-grained algorithm was used to match the surface shapes of the A β_{10-35} monomers. The next step was to refine the decoy sets and to obtain the dimer structures of lowest energy corresponding to each set. The structure of the A β_{10-35} was used to generate two homodimer decoy sets by maximizing the contact between the monomer surfaces. A shape-complementarity based algorithm, GRAMM,²⁴ was employed to create the decoy sets. The first 2000 dimer structures of each set were selected by minimizing the interaction energy between the monomers. Two expressions of the interaction energy were used. One function computes the desolvation energy of the buried residues at the dimer interface. The second scoring function added to the desolvation energy the contributions of the van der Waals and electrostatic intermonomeric interactions.

The dimer selected by a method that minimizes the desolvation energy of the residues at the dimer interface is referred to as the " ϕ -dimer". The dimer selected by minimizing the intermonomeric electrostatic energy is referred to as the " ϵ -dimer". The structure of the ϕ -dimer is dominated by contacts between hydrophobic segments of the monomers. The hydrophobic core, LVFFA(17-21), and the hydrophobic C terminus of both monomers are buried at the dimer interface. The contacts at the interface of the ϕ -dimer are conserved over the

lowest energy dimer structures. The ϵ -dimer interface is characterized by electrostatic intermolecular interactions, among which the salt-bridge Glu11(A)-Lys28(B) has the largest contribution. Contrary to the ϕ -dimer, the contacts observed at the ϵ -dimer interface are not conserved across the set of the low energy dimers due to the increased specificity and strength of the electrostatic interaction.

Computation of dimer association PMF

Starting from these two structures, we used classical molecular dynamics simulation to compute the potential of mean force (PMF)²⁵ and to study the stability of the two dimers and the structural fluctuations of the monomers within the stable dimer. The PMF as a function of the distance between the centers-of-mass of the two monomers was computed for both the ϕ -dimer and ϵ -dimer using the umbrella sampling method.²⁶ A higher free energy barrier characterizes the association process which leads to the ϵ -dimer, making the process leading to the ϕ -dimer more energetically favorable. The ϕ -dimer has a broader free energy minimum at the contact of the monomers, allowing larger fluctuations. Those fluctuations lead to entropic stabilization of the ϕ -dimer relative to the ϵ -dimer.

Probing the stability of the putative dimer structures

The stability of the putative ϕ and ϵ -dimer structures was analyzed through equilibrium molecular dynamics simulation. The distribution of the surface area buried at the interface of the monomers within the two dimer structures indicates that the ϕ -dimer structure is stable while the ϵ -dimer structure is not. The structural changes of the monomers within the ϕ -dimer were analyzed. The large value of the root-mean-square displacement (RMSD) from the initial ϕ -dimer structure of the A and B monomers indicates that the structures of both monomers are largely distorted from the initial collapsed coil conformation. However, monomer A is more distorted than monomer B. The structure of the hydrophobic core, LVFFA(17-21), is conserved during the simulation.

The results are presented in detail in the remainder of this section while a description of the computational methods used in this work is provided in Computational Model and Methods.

Generation of dimer structures

Dimer decoy discrimination using desolvation energy

The program GRAMM²⁴ was used to generate multiple dimer decoy structures based on shape complementarity. The best 2000 decoys were refined by minimizing the desolvation energy

computed using an atomic contact energy estimate:²⁷

$$S_{\phi} = \Delta E_{\text{desolv}} = \sum_{i=1}^{18} \sum_{j=1}^{18} e_{ij} n_{ij} \quad (1)$$

where e_{ij} is the work necessary to bring into contact two atoms i and j and n_{ij} is the number of the i - j contacts at the intermolecular interface within a 6.0 Å cutoff (see equation (4)). As the dimer is selected by a method that places a relative emphasis on the burial of hydrophobic residues at the dimer interface, it is referred to as the “ ϕ -dimer”. In

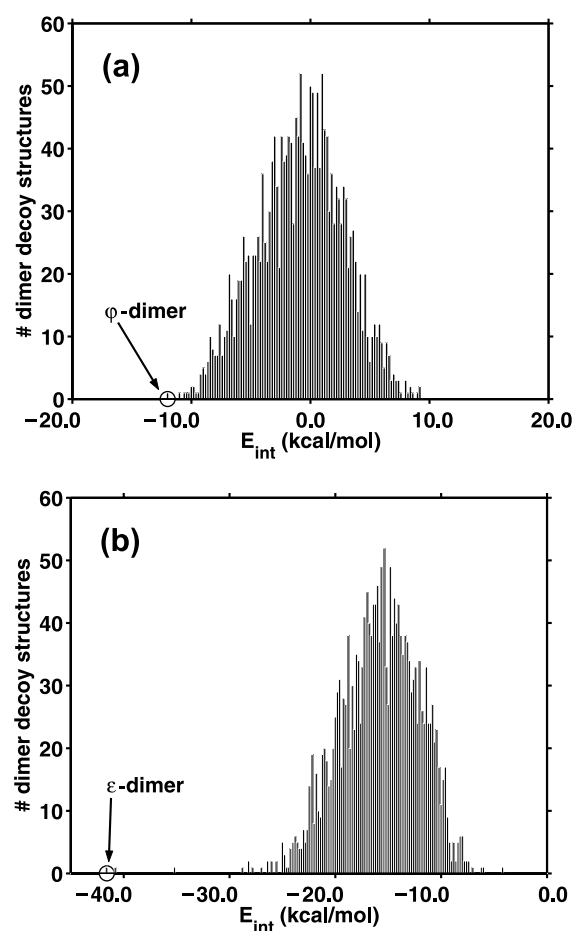


Figure 1. The distribution of the energy of interaction of the two monomers, used as the scoring function to analyze two sets of 2000 dimer decoys each. The dimer selected by a method that places a relative emphasis on the burial of hydrophobic residues at the dimer interface is referred to as the “ ϕ -dimer” (a). The dimer chosen by a method that places a relative emphasis on electrostatic interactions is referred to as the “ ϵ -dimer” (b). The “desolvation energy”, corresponding to the energy change on going from separated monomeric A β_{10-35} to A β_2 dimeric decoy structure, was used as a measure of the degree of hydrophobic surface burial. The decoy sets were obtained using two shape complementarity protocols, GRAMM (a) and ZDOCK (b). The energy of desolvation was calculated based on an atom contact energy (ACE) method. A bin of 0.2 kcal/mol was used to compute the distribution of the interaction energy.

Figure 1(a), the desolvation energy distribution corresponding to different dimer structures is presented. The configuration space is equally populated around the neutral desolvation. The lowest energy is -11.9 kcal/mol and the corresponding structure is presented in Figure 2(a), where only the residues at the interface are presented. Two side-chains, belonging to the monomer A and B, respectively, are at the dimer interface if the distance between their geometric centers is less than 6.5 Å. This is the dimer complex that was employed as the starting configuration in the PMF calculation and stability analysis. The magnitude of the desolvation energy is primarily determined by the hydrophobic–hydrophobic inter-monomer contacts. The hydrophilic residues in contact at the interface contribute to the overall

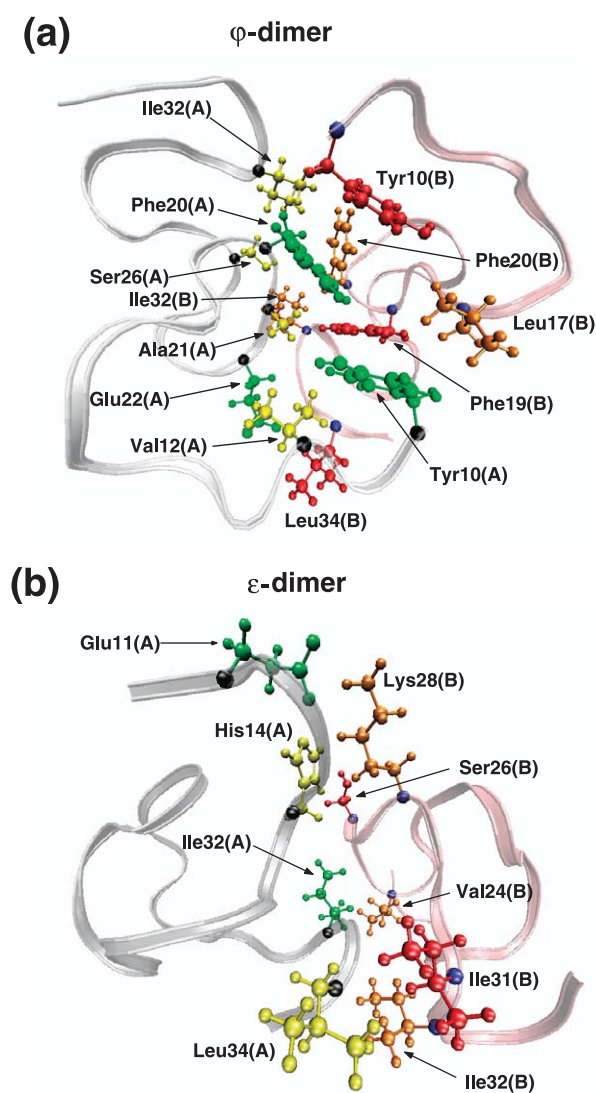


Figure 2. The putative dimer structures derived by minimization of the functions S_ϕ (equation (1)) and S_ϵ (equation (3)), corresponding to the ϕ -dimer (a) and ϵ -dimer (b), respectively. The side-chains at the dimer interface are depicted explicitly. The green and yellow colored residues belong to monomer A (left) and those in red and orange are part of monomer B (right).

stabilization of the dimer through the desolvation of their hydrophobic atoms. The unfavorable change in energy associated with the burial of the polar residues does not influence dramatically the value of the desolvation energy. In order to analyze the separate contribution of each of the monomers, we grouped the residues present at the interface in five motifs: the N terminus (first four residues, YEVH(10-13)), the central hydrophobic core (LVFFA(17-21)), a negative charged region (ED(22-23)), a β -turn sequence, VGSN(24-27), and the C terminus (the last five residues, IIGLM(31-35)). These motifs were chosen based on their proposed roles in contributing to the stability and activity of the A β_{10-35} .^{22,28} We let (A) and (B) stand for monomer A and monomer B, respectively.

The N terminus(A) is in contact with the hydrophobic core of monomer B, LVFFA(B). The contribution to the desolvation energy is -2.3 kcal/mol, and the inter-residue contacts are Tyr10(A)-Leu17(B) and Tyr10(A)-Phe19(B). In the dimer structure, the hydroxyl group of Tyr10 is exposed to solvent. At the same time, the N terminus(A) makes good contact with the C terminus(B), leading to a significant stabilization of the dimer structure. There are 116 atomic contacts between these two segments, although there is only one inter-residue contact, Val12(A)-Leu34(B), and the contribution to the desolvation energy is -3.3 kcal/mol. Subsequently, the hydrophobic contribution of the N terminus(A) to the dimer stability accounts for 47% of the total desolvation energy. The hydrophobic core of monomer A makes contacts with the N terminus(B) (-1.9 kcal/mol), the hydrophobic core of monomer B (-1.8 kcal/mol), and the C terminus(B) (-0.8 kcal/mol). Glu22(A) is in contact with Leu34(B), contributing unfavorably ($+0.2$ kcal/mol) with the C terminus(B). The β -turn of monomer A makes an energetically neutral ($+0.07$ kcal/mol) contact with LVFFA(B) through Ser26(A)-Phe20(B). The same region of monomer A touches favorably (-0.4 kcal/mol) the C terminus of monomer B, having one inter-residue contact, Ser26(A)-Ile32(B). Finally, the C terminus(A) is in the proximity of the N terminus(B) (-0.7 kcal/mol) and LVFFA(B) (-0.9 kcal/mol), having an interresidue contact Ile32(A)-Phe20(B). The residues involved in contacts at the dimer interface are identified in Figure 2(a).

Figure 3(a) depicts how the desolvation energies are dispersed over the distribution of the 2000 dimer decoy structures. We calculated the backbone RMSD of the decoy set from the structure corresponding to the minimum desolvation energy. In Figure 3(a), the distribution of desolvation energy as a function of RMSD is represented. Note that most of the dimer decoy structures are dissimilar to the structure of lower energy. The distribution shows a distinct “funnel-like” character, indicating that structures more similar to the reference structure tend to be structures of minimal energy. Analyzing the side-chain–side-chain contact

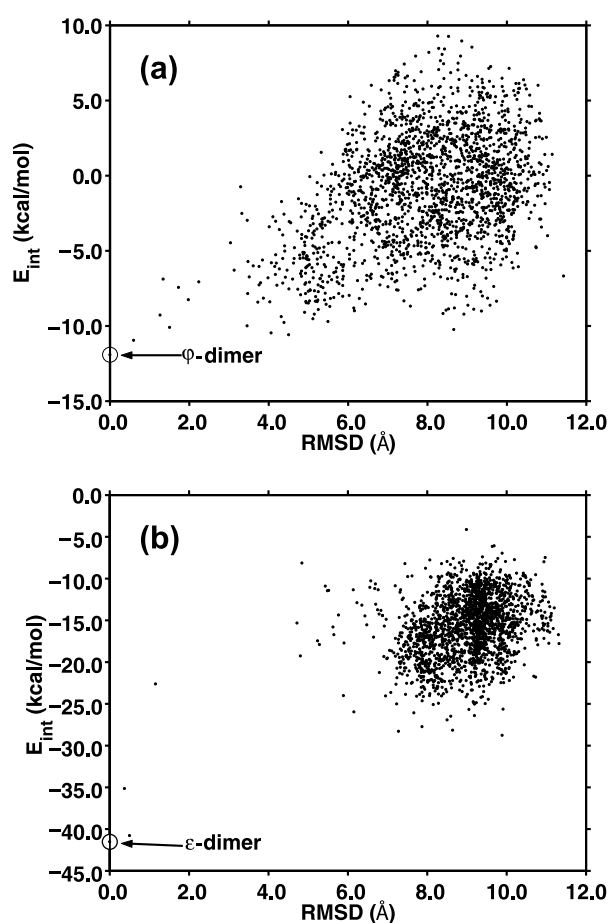


Figure 3. The distribution of the intermonomeric interaction energy plotted as a function of the atomic root-mean-square distance between each decoy structure and the structure of the ϕ -dimer (a) and the ϵ -dimer (b). In general, the unfavorable dimer structures are well differentiated from the most favorable structures. The desolvation energy distribution (a) has a “funnel-like” character, indicating that structures more similar to the reference structure tend to be structures of minimal energy. The contribution of the electrostatic interaction energy determines a discontinuous distribution (b), the structure of most of the decoy dimers being very different from the structure of the ϵ -dimer.

matrices for the structures found of greatest solvation energy, conserved structural elements can be identified (data not shown). Even though the contacts between the monomers are conserved, the value of the distance between the monomers may vary. This leads to relative deviations from the chosen ϕ -dimer structure. Additionally, the desolvation energy characterizes weak and largely unspecific interactions. The final magnitude of the desolvation energy corresponding to the ϕ -dimer is given by the large number of the hydrophobic contacts at the interface, contacts that are preserved for the lowest energy dimer structures. In contrast, the electrostatic interactions, which are more specific and stronger than the hydrophobic interactions, lead to a distribution that is more strongly peaked.

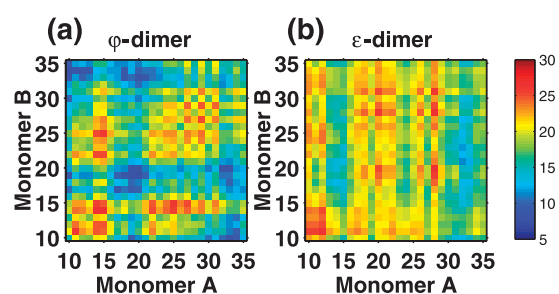


Figure 4. The side-chain-side-chain contact matrices averaged for the ten decoy structures corresponding to the ϕ -dimer (a) and ϵ -dimer (b), respectively. The selection of the ϕ -dimer is produced by a scoring function which is composed by the desolvation energy only (a), while the ϵ -dimer is selected by a function defined as the sum of the desolvation energy, the van der Waals and the electrostatic interactions (b) (see the text for details). The interface of the ϕ -dimer is dominated by contacts which involve hydrophobic residues, while the presence of the polar and charged residues is evident at the interface of the ϵ -dimer. The amino acid sequence of the A β_{10-35} monomer is Y¹⁰EVHHQ¹⁵KLVFF²⁰AEDVG²⁵SNKGA³⁰IIGLM³⁵.

Since the contacts between the monomers of the ϕ -dimer are conserved for the lowest energy structures, especially those involving hydrophobic residues, we can say the chosen ϕ -dimer is representative for the dimer decoy set refined with a scoring function which places a relative emphasis on hydrophobicity at the dimer interface. Due to the absence of any experimental initial structure of the A β_{10-35} dimer, it is difficult for us to identify the biological relevance of the initial ϕ -dimer. However, the contacts between the hydrophobic residues are in agreement with the experimental observation that the hydrophobic force may contribute significantly to the dimerization (e.g. through studies of the F19T mutant of A β -protein^{29,30}).

In order to keep a simplified representation, the inter-monomer side-chain contacts, corresponding to the ϕ -dimer averaged for the ten decoy structures, are shown in Figure 4(a). The most evident conserved structural elements are found in the LVFFA(A)–LVFFA(B) contacts. In addition, the N terminus(A)–C terminus(B), LVFFA(A)–C terminus(B), and the C terminus(A)–N terminus(B) contacts are well preserved, with the sole exception of the fifth dimer. For that structure, the N terminus(A)–C terminus(B) and the C terminus(A)–N terminus(B) are shifted to C terminus(A)–C terminus(B). The N terminus(A)–LVFFA(B) contact, which is presented in the first, second and the sixth structures, is diminished in favor of the C terminus(A)–LVFFA(B) proximity (data not shown).

Dimer decoy discrimination using electrostatic energy

The program ZDOCK 2.3³¹ was used to generate 2000 dimer decoy structures of A β_{10-35} . The scoring

function is given by the weighted sum³² of the shape complementarity, S_{sc} , desolvation energy, S_{ds} , and electrostatic interaction energy, S_{elec} :

$$S_{ZDOCK} = a_1 S_{sc} + S_{ds} + b_1 S_{elec} \quad (2)$$

where $a_1=0.01$ and $b_1=0.06$. The shape complementarity and the desolvation energy computation involved the same protocols as those corresponding to the GRAMM program. The electrostatic interaction is the coulombic energy between the two dimers. The set of the dimer structures was further refined using a scoring function given by the sum of the van der Waals energy between the two dimers, desolvation energy of the dimers, and the electrostatic interaction energy:

$$S_\varepsilon = S_{vdw} + S_{ds} + b_2 S_{elec} \quad (3)$$

where $b_2=0.5$. The value of b_2 corresponds to a dielectric constant of 2, characteristic of the predominantly non-polar protein interior. The choice of $b_2=0.5$ was made for two reasons. The first was to enhance the stability of that dimer structure in which the electrostatic interaction is a major contribution to the scoring function. Secondly, we wished to adjust the electrostatic and the van der Waals energies to be of the same order of magnitude. The motivation for including the van der Waals energy in the scoring function was to maximize the contact surface at the interface.

The distribution of the scoring function over the decoy set is presented in Figure 1(b). Contrary to the previous case, in which the scoring function was based on the desolvation energy alone, here all computed energies are negative, all dimer decoy structures are energetically stable compared with the separated monomers. The value of the interaction energy corresponding to the most probable dimer structure obtained in this way is -41.5 kcal/mol. The prefactor b_2 is included in this value. The contribution of the electrostatic interaction is -21.9 kcal/mol, the van der Waals energy is -18.2 kcal/mol, while the desolvation energy is only -1.4 kcal/mol. The dimer structure corresponding to the lowest energy is depicted in Figure 2(b). As the dimer is chosen by a method that places a relative emphasis on electrostatic interactions, it is referred to as the " ε -dimer". In order to characterize the residue composition of the dimer interface, we defined a contact between two side-chains to exist if the distance between their geometric centers is less than 6.5 Å. There are six contacts at the dimer interface. The contact that makes the largest contribution to the scoring function is Glu11(A)-Lys28(B), which is a salt-bridge contributing -37.7 kcal/mol to the total electrostatic interaction energy. In the same region, one can observe contacts between His14(A) and Lys28(B) (-3.2 kcal/mol contribution to the electrostatic energy), and His14(A) with Ser26(B) (only -0.5 kcal/mol electrostatic contribution). The C terminus(A) is in contact with the β -turn(B) through the contact Ile32(A)-Val24(B). Also, the C terminus(A) is in the proximity of the C terminus(B),

making two contacts, Leu34(A)-Ile31(B) and Leu34(A)-Ile32(B). The favorable desolvation energy as determined by the hydrophobic contacts, in which the C terminus(A) is involved (-2.3 kcal/mol), is reduced because of the contacts made by Lys28(B) ($+1.0$ kcal/mol).

In Figure 3(b), the interaction energy as a function of RMSD from the most favorable dimer structure is presented. There are three structures within 1.0 Å atomic RMSD, one structure with the atomic RMSD between 1.0 Å and 2.0 Å, and the rest of the dimers have the atomic RMSD greater than 4.0 Å. One can observe the lack of any structure between 1.5 Å and 4.0 Å, contrary to the case in which the scoring function was entirely based on the desolvation energy. Analyzing the contact maps, major differences between the peptide-peptide contacts in the ten lowest energy dimer structures are observed (data not shown). In order to maintain a simplified representation, we depicted the intermonomer side-chain contacts in Figure 4(b) corresponding to the ε -dimer averaged for the ten decoy structures. Contrary to the averaged contacts corresponding to the ϕ -dimer, there are no deep minima in the averaged contact matrix of the ε -dimer. This is caused by the large heterogeneity of the first ten ε -dimer decoys. As seen in Figure 4, the averaged contact maps show that the ϕ -dimer contacts are distinctly symmetric, while the ε -dimer contacts are as distinctly asymmetric. These symmetry properties are also evident in the individual contact maps for the sets of ten ϕ and ε -dimers. The first three decoys of the ε -dimer are practically identical. The predicted stability of those structures is almost entirely due to the favorable electrostatic interaction resulting from the salt-bridge Glu11(A)-Lys28(B). The contributions of the van der Waals and the desolvation energies play no role in the discrimination of these configurations. The fourth decoy is stabilized by the favorable van der Waals interaction (-16.7 kcal/mol), while the electrostatic interaction is substantially smaller (-6.4 kcal/mol), being comparable to the desolvation energy (-5.6 kcal/mol). This increased value of the desolvation energy is a result of hydrophobic contacts, similar to the GRAMM-generated decoy set. In the fourth dimer structure, contacts between LVFFA(A)-LVFFA(B), LVFFA(A)-C terminus(B), C terminus(A)-LVFFA(B), and C terminus(A)-C terminus(B) are present. The most favorable van der Waals interaction energy corresponds to the sixth decoy (-21.6 kcal/mol), while the electrostatic interaction for this structure is only -2.2 kcal/mol, lower than the desolvation energy (-4.4 kcal/mol). This observation lends support to the idea that, in the case of A β_{10-35} dimer, a large surface area contact between the two monomers will correspond to a low electrostatic interaction. For the remaining decoys, the van der Waals interaction plays the principal role in discrimination (between -17.5 kcal/mol and -20.3 kcal/mol), with the electrostatic interaction (between -2.0 kcal/mol and -3.0 kcal/mol) representing a smaller

contribution to the desolvation energy (between -4.0 kcal/mol and -4.6 kcal/mol).

Potential of mean force

The PMF computed along the distance between the centers-of-mass of the two monomers is plotted in Figure 5. The PMF corresponding to the dimerization process was computed initiating the calculation with the monomers "in contact" in a dimer structure and then drawn gradually outward, in 0.5 Å steps followed by substantial configurational sampling, by means of the umbrella sampling constraint. The PMF was computed independently from two initial dimer structures represented in Figure 2 and described in detail in the previous section. Briefly, one putative dimer structure (shown in Figure 2(a)) was determined to be the most stable of 2000 dimer decoy structures using an estimate of the free energy of association based on a contact potential estimate of the solvation energy (equation (1)). The second putative dimer structure (shown in Figure 2(b)) was determined to be the most stable of 2000 dimer decoy structures where the estimate of the free energy of association was a weighted sum of the van der Waals, electrostatic, and atomic contact solvation energy potentials (equation (3)). The structure resulting from the selection based on the shape complementarity and stabilization estimated by desolvation potential emphasizes hydrophobic contacts and burial of hydrophobic surface and will be referred to as the ϕ -dimer. The second structure

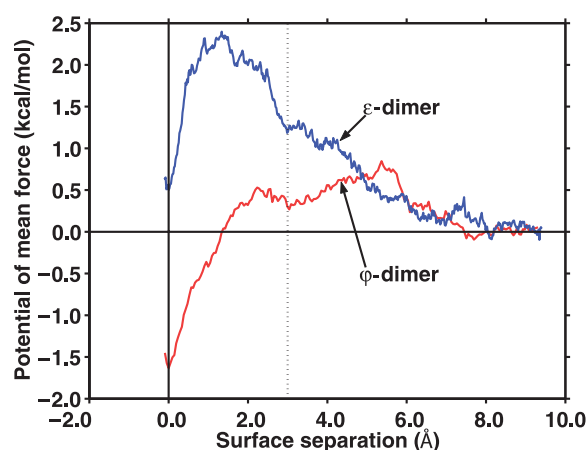


Figure 5. The PMF is plotted for two different relative orientations of the monomeric peptide within the dimer. The PMF is computed as a function of the surface separation, $\delta = \xi - \xi_{\text{cont}}$, along the distance between the centers-of-mass (DCOMs) of the two monomers, where ξ and ξ_{cont} are the DCOMs of the two monomers when they are at an arbitrary separation and in contact, respectively. The profile in blue corresponds to the free energy surface computed using the ϵ -dimer as the starting structure. The red curve is similarly computed using the ϕ -dimer as the starting structure. The difference between the two surfaces suggests that hydrophobic interactions may be more essential to stabilization of the dimer structure than electrostatic interactions.

selected for shape complementarity and burial of hydrophobic residues, but placing a greater emphasis on the relative importance of electrostatic interactions, is referred to as the ϵ -dimer. Both free energy profiles were shifted so that the value of the PMF is zero at the maximum separation.

For each free energy profile, one can distinguish three distinct intervals. In the outer interval, the PMF value is nearly constant, from 6.5 Å– 7.0 Å to maximum separation, which in our case is 9.0 Å. At a distance of 6.5 Å for the ϵ -dimer and 7.0 Å for the ϕ -dimer, the first solvation shells of the monomers come into contact, and for both dimers the energetics of desolvation of the associating monomers is unfavorable. In the second interval for the ϵ -dimer, the value of the PMF continues to increase up to 1.2 kcal/mol at a 3.0 Å separation; for the ϕ -dimer, the potential energy reaches a value of 0.8 kcal/mol at 5.5 Å, and after that the desolvation is favorable, ending in an unstable local minimum at 3.0 Å. For the third interval, from 3.0 Å to 0.0 Å, there is only one solvation shell between the monomers. The water molecules are most strongly ordered near the monomers through electrostatic interactions and hydrogen bonds. As a result, the PMF for the ϵ -dimer increases sharply between 3.0 Å and 1.3 Å up to 2.4 kcal/mol. At contact, the van der Waals attraction predominates, making the overall dimerization process energetically favorable. For the ϕ -dimer, the solvation shell between the hydrophobic regions of the monomers is only weakly bound to the solute, and after a small increase in the PMF, corresponding to the van der Waals attraction, the desolvation is entirely favorable.

Comparing these two extreme models for monomer association, one which supposes that the principal mechanism stabilizing the dimer structure is the burial of hydrophobic surface, leading to the ϕ -dimer, and another that supposes that the electrostatic interaction is the primary associative stabilizing interaction leading to the ϵ -dimer, it can be observed that the former appears to lead to more energetically favorable dimerization than the latter. It appears to be more efficient to remove the entropically unfavorable structured water between the opposing hydrophobic regions of the two monomers than to stabilize the monomer solely through electrostatic interactions. This is in good agreement with the experimental observation that the mutation E22Q, where a charged glutamic acid residue is replaced by a polar glutamine residue, increases the propensity for amyloid formation.^{23,33} Massi & Straub, using molecular dynamics simulation, studied this increased amyloidogenic activity for the E22Q mutant peptide. One of their conclusions was that the water-peptide interaction is less favorable for the mutant peptide than for the WT peptide.³⁴ Following a more detailed analysis of the structure and dynamics of the WT and E22Q A β_{10-35} , Massi *et al.*³⁴ suggested that a change in the charge state of the peptide, due to the E22Q mutation, leads to an increase of the

hydrophobicity of the peptide that could be responsible for the increased activity.¹²

Stability of dimer

The structures of φ and ε -dimers were used as the initial structures in five “independent” 10 ns NPT molecular dynamics simulations for each dimer structure. The trajectories were initiated from the same point in configurational space, corresponding to the φ and the ε -dimers, and using different starting points in velocity space. Due to the complexity of the system, the five trajectories proved to be highly uncorrelated from the beginning of the simulations. The goal of these simulations was to study the stability of the putative φ and ε -dimer structures in the absence of restraints. As a measure of the stability of the dimer structure, we computed the surface area buried at the interface of the two monomers, and its evolution in time is plotted in Figure 6. The area buried at the interface represents the fragment of the total surface of the dimer which is not exposed to the solvent.

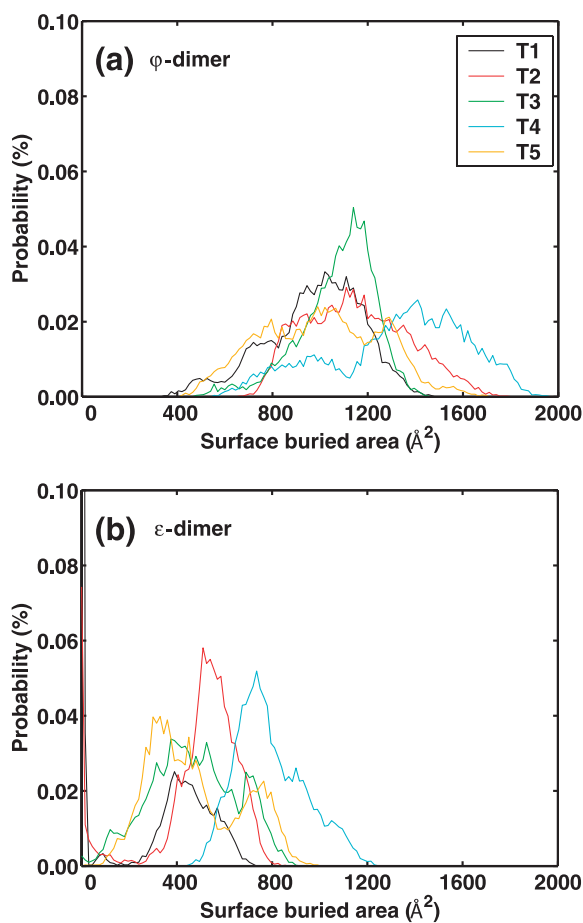


Figure 6. The distribution of the surface buried area at the interface between the $A\beta_{10-35}$ monomers during the molecular dynamics simulation of the dimer indicates that the set of the principal contacts at the dimer interface are maintained for the φ -dimer (a), and that the ε -dimer is not stable (b). A bin of 15 Å was used to compute the distribution of the interface surface area.

The solvent exposed surface area was computed using the method of Lee & Richards.³⁵ Essentially, a probe sphere, with a radius of 1.4 Å, is swept on the van der Waals surface to define the solvent exposed surface. The initial values of the buried surface areas at the interface are 895.0 Å² and 606.2 Å² within the φ and the ε -dimers, respectively. In Figure 6(a), it can be observed that the monomers within the φ -dimer are in permanent contact during the course of the simulation. Comparing the contribution to the total energy interaction between the two monomers within the φ -dimer of both the electrostatic energy and the desolvation energy of the interface, (Figure 7), we observe that the stability of the φ -dimer is determined by the hydrophobic interaction between the monomers. However, there are two situations where the contribution of the electrostatic interaction transiently exceeds the effect of burying hydrophobic residues at the interface. A first electrostatic “spike” is observed in the fourth trajectory, T4, where a salt-bridge Lys16(A)-Glu11(B) is formed in the time interval 7.2–8.0 ns. A second electrostatic spike occurs in the fifth trajectory, T5, where Lys16(B) is located between Glu22(A) and Asp23(A) in the time interval 8.2–9.6 ns. In both cases, the salt-bridges have a short life time relative to the simulation time, due to the screening effect of the solvent, which reduces the strength of the electrostatic interaction. In fact, due to the size of the monomer (only 26 residues), all residues “buried” at the interface of the dimer will be in contact with the solvent. For a short peptide, it is difficult to define an “interior” because almost all the residues will have a contact surface with the solvent. Even for the dimer, the residues at the interface are not totally buried and are partially exposed, to some extent, to the solvent. In the case of a folded protein, which is a macromolecular structure with hundreds of residues, there is a well-defined interior, in the sense that there are hydrophobic residues fully covered by other residues. In general, the hydrophobic character of the folded protein interior favors an α -helical organization of the residues buried. Using geometric arguments (cubic lattice), one may expect an interior for $A\beta_{1-42}$. However, the $A\beta_{1-42}$ is still a small protein and we consider that the definition of a strict interior will be difficult. The seven hydrophobic residues added at the C terminus of the $A\beta_{10-35}$ cannot be covered by nine, supposedly highly flexible, residues added at the N terminus. In fact, the major obstacle in obtaining a 3D structure for the $A\beta_{1-42}$ is the high flexibility of the termini in an aqueous solvent. We speculate that there will be little difference between the $A\beta_{1-42}$ and $A\beta_{10-35}$ proteins in terms of defining an interior. The electrostatic interaction energy was computed by solving numerically the Poisson equation using the PBEQ module³⁶ implemented in the biomolecular simulation program CHARMM. We used a relative dielectric constant of 80 for water and 2 for the interior of the monomers. The contribution of the hydrogen bonds to the stability of dimer is included

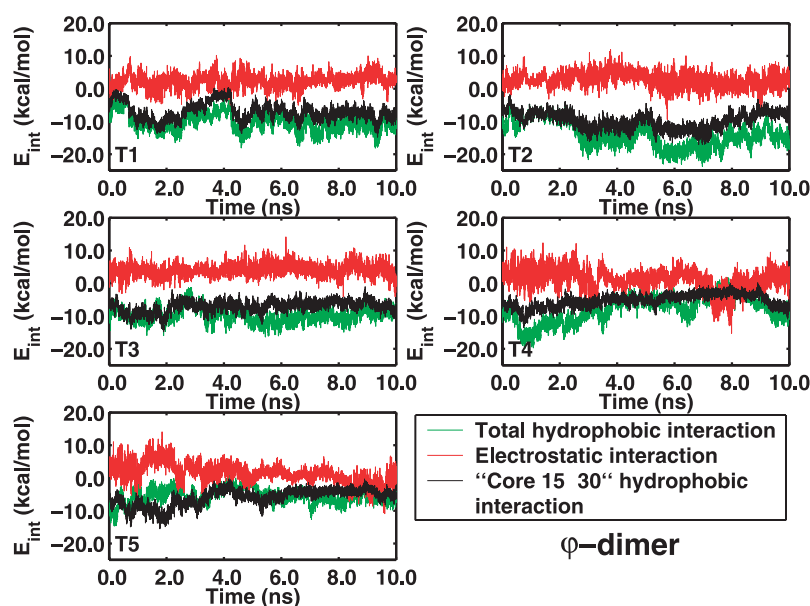


Figure 7. The comparison of the electrostatic (red) and the hydrophobic (green) interaction energies between the $A\beta_{10-35}$ monomers during the molecular dynamics simulation implies that the stability of the ϕ -dimer is given by contacts between hydrophobic residues. In black is shown that the contribution of the core 15–30 plays a dominant role to the overall stability of the ϕ -dimer.

in the electrostatic interaction. The desolvation energy was computed using the ACE algorithm (see Computational Model and Methods), and was used here as a measure of the hydrophobic interaction between the two monomers of the ϕ -dimer.

The favorable contribution to the hydrophobic interaction energy is conferred by the hydrophobic residues involved at the interface. The residues in contact at the interface of the ϕ -dimer at the beginning of simulation are shown in blue in Figure 4(a). It can be observed that the “extended core” region 15–30 of both monomers, and specifically the hydrophobic core LVFFA(17–21), is involved at the interface of the ϕ -dimer. We computed the role of the fragment 15–30 to the stabilization energy, assuming that at least one monomer contributes with its extended core at the interface. In Figure 7, in black, it can be observed that the fragment 15–30 makes a dominant contribution to the ϕ -dimer. The small value of the difference between the hydrophobic energies of the entire dimer and the “reduced” dimer structure, containing at least one fragment 15–30 at the interface, suggests that the initial contacts N terminus(A)–C terminus(B) and C terminus(A)–N terminus(B) do not have an important contribution to the dimer stability.

Massi *et al.*²⁸ showed that, in the monomeric peptide, fluctuations of the N and C termini are larger than those observed in the rest of the peptide, in agreement with NMR studies of the $A\beta_{10-35}$ in aqueous solution.²⁸ The similar large conformational fluctuations of the N and C termini in both the ϕ and ε -dimer structures suggest that there is a small contribution to the dimer association free energy contribution associated with those terminal regions of the peptide.

In Figure 6(b), the evolution of the interface surface area presents evident signs of instability for

the ε -dimer. The structure of the ε -dimer was determined by allowing the electrostatic interaction energy between the monomers to play an important role in the overall interpeptide interaction energy. An essential interaction that determines the structure of the ε -dimer is the Glu11(A)-Lys28(B) salt-bridge. However, because Glu11(A) and Lys28(B) are highly exposed to solvent, their electrostatic interaction will be screened by solvent, and thus, their contribution to the stability of the ε -dimer will be dramatically reduced. For example, for the first trajectory T1, shown in Figure 8, the salt-bridge Glu11(A)-Lys28(B) is disrupted after 1.4 ns. During the next 2.6 ns, both monomers reorganize at the interface, in order to stabilize the dimer through hydrophobic contacts formed by Leu17(A), Leu34(A), Met35(A), Val12(B), Ile31(B), and Ile32(B). However, after 4 ns from the beginning of the simulation, both monomers are completely separated. A similar scenario is observed for T2, with the difference that the dimer is disrupted faster; after 0.4 ns there is no contact surface at the interface. However, after 1 ns of separation, the monomers rotate relatively one to the other, and the hydrophobic C terminus(A) makes contacts with the hydrophobic core LVFFA(17–21)(B) and C terminus(B), resulting in a relatively stable dimer. For the third trajectory, the Glu11(A)-Lys28(B) salt-bridge is broken after 0.3 ns, and, for the next 1.6 ns, the stability of the dimer is assured by the contacts at the C terminus(A)–C terminus(B) region. After 1.9 ns from the beginning of the T3 trajectory, the salt-bridge Glu11(A)-Lys28(B) is reformed. Its relative stability favors increased contacts between the C terminus(A)–C terminus(B) region. A consequence of the increasing hydrophobicity near the salt-bridge Glu11(A)-Lys28(B) is reflected in a lower local dielectric constant. This effect contributes to the stability of the salt-bridge. However, due to the large fluctuations in the C termini regions, after

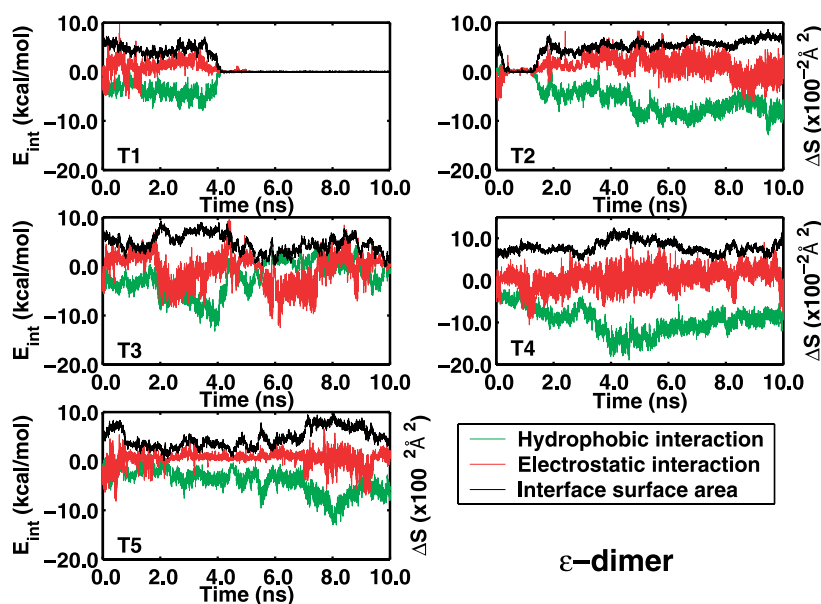


Figure 8. The comparison of the electrostatic (red) and the hydrophobic (green) interaction energies between the $A\beta_{10-35}$ monomers during the molecular dynamics simulation implies that the stability of the ϵ -dimer cannot be assured by the electrostatic interaction between the monomers, and that the ϵ -dimer tends to reduce the exposure to solvent of the hydrophobic residues. The behavior of the interface surface area (black) implies that the ϵ -dimer is not stable in the first three trajectories (T1, T2, and T3). For the remaining two (T4 and T5), it appears that the reorganization of the interface, by reducing the unfavorable exposure of the hydrophobic residues to the solvent, stabilizes the ϵ -dimer. Due to the screening effect induced by the polar solvent, the strength of

the transient interpeptide salt-bridges is reduced, and, thus, the electrostatic interaction between the monomers cannot assure the stability of the ϵ -dimer.

4.0 ns the salt-bridge Glu11(A)-Lys28(B) is broken again. Asp23(A) is involved in electrostatic interaction, initially with Lys16(B) and continuing with Lys28(B) (5.5–7.5 ns), with the same destabilizing influence due to the dielectric screening by the solvent. A last salt-bridge is formed between Lys16(A)-Asp23(B), and after 11.0 ns from the beginning of the third trajectory, the monomers are completely separated. The next two simulations, T4 and T5, appear to generate more stable dimer trajectories. The stability of the dimer is indicated by an increased hydrophobic interaction between the monomers. These results suggest that the scoring function used to recognize the ϵ -dimer overemphasizes the importance of salt-bridge formation due to incomplete screening in the solvation of charged side-chains.

Dynamical fluctuations in the ϕ -dimer

As our analysis indicates that the ϵ -dimer structure is unstable, in the remainder of this section we analyze the structural changes of the monomers within the ϕ -dimer alone. The RMSD from the initial ϕ -dimer structure of the monomers A and B is displayed in Figure 9(a) and (b), respectively. The large value of the stabilization plateau (around 5.5 Å) indicates that, during the simulation, the structures of both monomers are largely distorted from the initial collapsed coil conformation. However, we can observe that monomer A is more distorted than monomer B. In Figure 9(c) and (d) is displayed the distribution of the RMSD from the initial structure of the hydrophobic core, LVFFA(17-21), of the monomers A and B, respectively. It can be observed that the displacements from the initial ϕ -dimer structure in the hydrophobic region are smaller than those corre-

sponding to the entire monomer. This is evidence that the peptide monomers preserve the structure of the central hydrophobic cluster, LVFFA(17-21), as observed for the monomeric peptide in experiment³⁷ and simulation.²⁸ The preservation of that core structure may play an important role in stabilizing the ϕ -dimer.

The distributions of the radius of gyration, R_g , are presented in Figure 10. The monomer A (Figure 10(a)) has a greater radius of gyration than the monomer B (Figure 10(b)), the latter monomer having a radius of gyration quite close to the average value. This difference is in accordance with the dissimilar RMSD profiles corresponding to the monomers A and B. The R_g value of monomer B is quite close to the value characteristic of the monomer ($\langle R_g \rangle = 9.2 \text{ \AA}$) simulated by Massi *et al.*²⁸ The end-to-end distance distributions shown in Figure 10(c) and (d) show substantial variations, and indicate that the monomers experience considerable reorganization in the terminal regions of the peptides within the simulated ensemble of dimer states, with the observation that the monomer A (Figure 10(a)), is more distorted compared to the monomer B (Figure 10(b)).

The structural fluctuations, characterized by the dynamics of the radii of gyration of the monomers in the homodimer, are asymmetric (see Figure 10(a) and (b)). Such asymmetric fluctuations may be related to the intrinsic heterogeneity in the interpeptide and peptide-water interactions. The fluctuations in the hydrophobic interface involving the residues in the central hydrophobic cluster, LVFFA(17-21), undergo minimal values. It follows that the large asymmetric fluctuations arise from interactions involving the rest of the molecule. The observed asymmetry may be related to the pathways followed in the assembly and disruption of

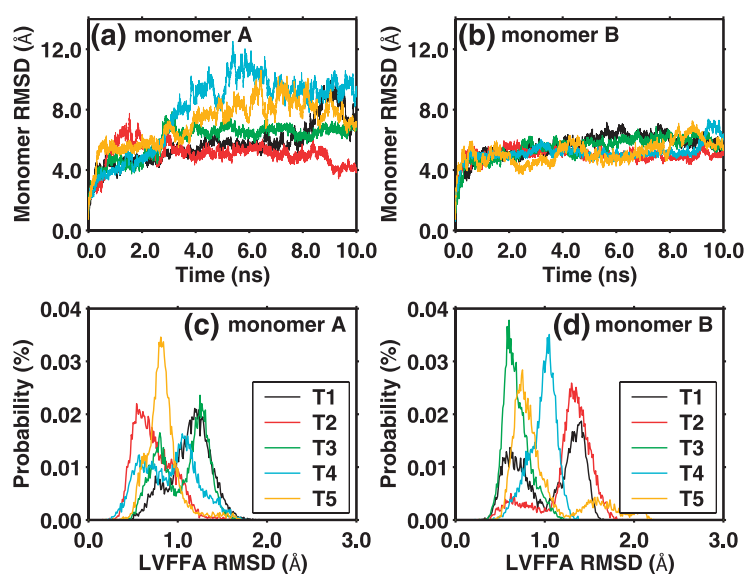


Figure 9. The root mean square displacement of the entire $A\beta_{10-35}$ fragment for the monomers A (a) and B (b) during the NPT molecular dynamics simulation, in the absence of restraints, indicates that the monomers undergo reorganization from the initial dimer configuration. Under the same conditions, the distribution of the RMSD of the hydrophobic fragment LVFFA(17-21) suggests a more conservative structure for both monomers A (c) and B (d). A bin of 0.01 Å was used to compute the distribution of the LVFFA RMSD.

the homodimer. Using lattice models, it has been shown that there are multiple routes in the formation of homodimers that are stabilized by hydrophobic contacts at the interface. A corollary of this finding is that even after dimerization, the individual monomers can sample different conformations on a multitude of time-scales. Hydrogen exchange experiments of homodimers can be used to probe the extent of asymmetry in the fluctuations of the individual monomers.

Time dependence of secondary structure fluctuations in the homodimer

In order to further analyze the conformational changes of the two monomers, the time-evolution of

the secondary structure is plotted in Figure 11. An increasing percentage of the peptide structures with broad regions of the peptide having backbone conformations consistent with β -strand is observed. To some degree, the formation of β -strand structure appears to be preceded by the formation of α -helical structure. This is in qualitative agreement with the experimental observation of Kirkitadze *et al.*²⁰ who monitored the secondary structure of $A\beta_{1-40}$ and $A\beta_{1-42}$ during the incubation at pH 7.5 using circular dichroism (CD) spectroscopy and observed that the amount of β -strand increases after a transitory increase of the α -helix content. Of course, our observation is made with regard to local backbone fluctuations indicating the propensity for secondary structure formation on the time-scale

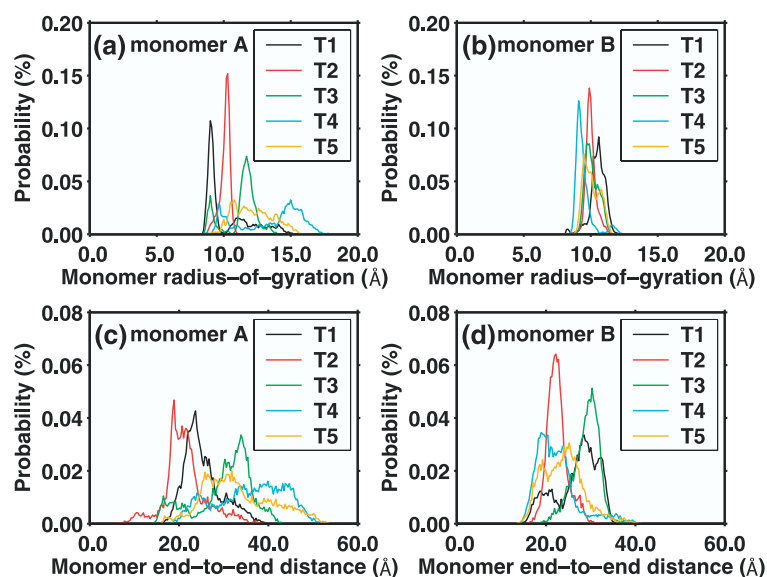


Figure 10. The distribution of the radius of gyration demonstrates that the collapsed coil structure, characteristic of the monomeric $A\beta_{10-35}$, as determined experimentally and through simulation analysis in aqueous solution,²⁸ is not preserved during the simulation of the dimer. The monomer A (a) appears to adopt a more extended conformation than that of the monomer B (b). The monomeric $A\beta_{10-35}$ end-to-end distance distribution demonstrates that the monomers experience considerable reorganization in structure over the course of the 10 ns NPT molecular dynamics simulation. The tendency of the monomer A (c) to have a more extended conformation compared with the monomer B (d) is evident. Bins of 0.1 Å and 0.3 Å were used to compute the distributions of the radius of gyration and end-to-end distance, respectively.

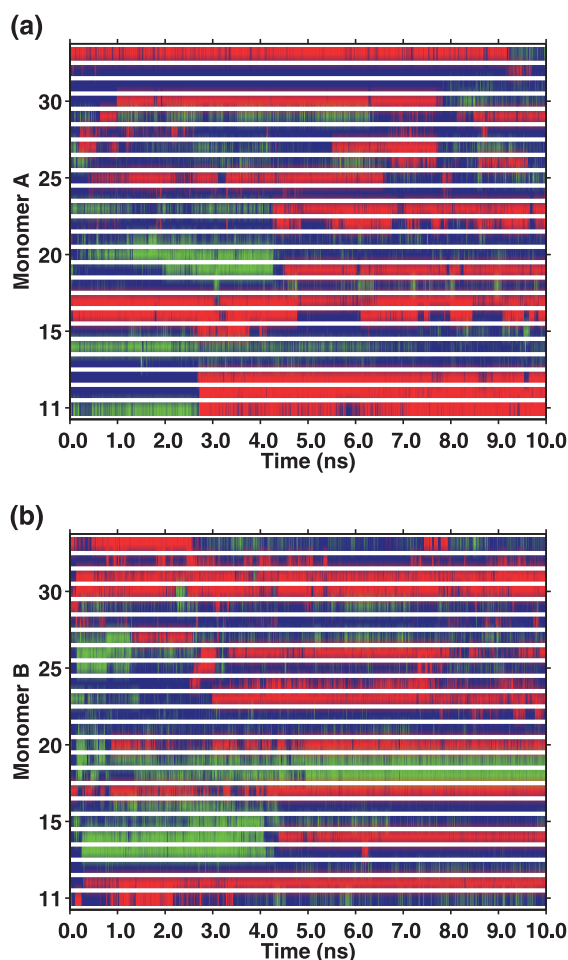


Figure 11. The time evolution of the secondary structure of monomer A (a) and monomer B (b), corresponding to the first trajectory T1 of the ϕ -dimer, shows strong signs of formation of β -strands preceded or accompanied by formation of trace amounts of α -helical structural motifs. Random coil is represented in blue, α -helical structure in green, and β -strand in red.

of nanoseconds, while the experiment observes the actual formation of secondary structure (as implied by CD spectra) on the time-scale of hours.

Summary and Conclusions

This study has examined the dimerization of the A β_{10-35} using three computational methods.

(1) The structure of the dimer was selected among a large number of relatively low-energy “decoy” configurations. The set of candidate dimer decoy structures was generated based on a shape-complementarity protocol, GRAMM. The structure supposed to be most stable was obtained by refining the list of candidates using an approximate desolvation energy discrimination. While the distribution of the desolvation energy over the dimer structures within the set indicates that the stable dimer structure is not entirely unique, all dimer

decoy structures showed similar characteristic residue–residue contacts at the dimer interface.

(2) Initiating the calculation from the contact structures for the ϕ and ϵ -dimers, molecular dynamics simulation was used with umbrella sampling to compute the PMF. The free energy profile corresponding to the process of dimerization governed by hydrophobic interaction between the monomers (ϕ -dimer) was compared with a behavior dominated by the electrostatic interaction between the peptide monomers (ϵ -dimer). In the former case, the energy required to remove the water between the monomers is comparable with the thermal energy scale, $k_B T$, at room temperature. In the latter case, the resistance to desolvation is approximately 2.5 kcal/mol, making the binding of the monomers less favorable. However, once the peptide desolvation is accomplished in each case, there remain significant differences in the peptide energetics. In the ϵ -dimer, the stabilization by electrostatic interactions leads to a positive (0.5 kcal/mol) binding free energy minimum, with the monomers in close contact, the value of the free energy decreasing sharply in a narrow region from 1.3 Å to the van der Waals contact, as can be observed in the PMF (Figure 5). For the ϕ -dimer, the stabilization by the burial of hydrophobic surface leads to a broader free energy minimum (−1.5 kcal/mol), allowing larger fluctuations within the dimer state ensemble. Those fluctuations result in an entropic stabilization of the peptide relative to the more specific and constrained electrostatic interactions stabilizing the ϕ -dimer. Widom *et al.*³⁸ estimated the free energy of the hydrophobic attraction to be on the order of $k_B T$, which is in good agreement with our computation.

(3) The putative ϕ and ϵ -dimer structures were simulated for 10 ns of NPT molecular dynamics. The time evolution of the ϕ -dimer structure was analyzed and it was observed that the monomers remain in contact during the simulation. It was shown that the hydrophobic interaction between the monomers of the ϕ -dimer acts as a stabilizing force of the dimer. The “extended core” region 15–30 of both monomers in the ϕ -dimer makes the principal contribution to the hydrophobic interaction energy. The ϕ -dimer undergoes internal structural reorganization in the terminal regions of the monomeric peptides. Our simulations indicate that there is substantial reorganization of the peptide monomers in the N and C terminus regions, as expected for a dimer weakly and relatively non-specifically stabilized by hydrophobic contacts at the dimer interface. Importantly, the structure of the central hydrophobic cluster LVFFA region assumes a conformation similar to that observed for the monomeric peptide in both experiment³⁷ and simulation.²⁸ Our simulations suggest that the preservation of the structure of the LVFFA central hydrophobic cluster plays an important role in the stabilization of the ϕ -dimer structure.

The structure of the ϵ -dimer is not stable during the molecular dynamics simulation. It appears that

the electrostatic interaction between the two monomers, which was used to determine the structure of the ϵ -dimer, does not act as a stabilization force. The solvation of salt-bridges formed at the interface increases the value of the local dielectric constant, decreasing the strength of the electrostatic interaction. In order to increase its stability, the ϵ -dimer tends to exaggerate the interpeptide hydrophobic interaction.

The finding that the φ -dimer may constitute the ensemble of stable A β_{10-35} dimer has important implications for fibril formation. The initial event in the dimerization involves, in all likelihood, contacts between the central hydrophobic clusters. In this process, expulsion of water molecules in the interface might be a key event just as in the oligomerization of A β_{16-22} fragments.²¹ Since this process involves cooperative rearrangement of ordered water molecules, it is limited by an effective free energy barrier. Based on our results, we form a conjecture that events prior to the nucleation process themselves might involve crossing free energy barriers which depend on the peptide-peptide and peptide-water interactions.

Computational Model and Methods

In the protocol for generating the decoy sets, the dimer structures were generated using a shape-complementarity-based algorithm. The dimer structures were discriminated by comparing estimates of the desolvation energy using an atomic contact energy protocol. Starting from the putative dimer structure, molecular dynamics trajectories were simulated with umbrella sampling to compute the PMF. The stability of the dimer structure was demonstrated through the computation of the PMF, which shows that the dimer represents a minimum in the free energy. The simulation of 10 ns trajectories further shows the stability of the contact dimer. The PMF and dynamical trajectories were analyzed and used to characterize the ensemble of peptide dimer configurations. The amino acid sequence of the A β_{10-35} is Y¹⁰EVHHQ¹⁵KLVFF²⁰AEDVG²⁵SNKGA³⁰IIGLM³⁵.

Dimer structure generation using a docking protocol

Decoy structures of the A β_{10-35} dimer were generated using the shape-complementarity-based algorithm Global Range Molecular Matching (GRAMM).²⁴ The surface of a macromolecular structure depends on the Cartesian coordinates of the atoms composing the macromolecule. The surface is not planar (bi-dimensional, N^2) but irregular, having a 3D profile. Consequently, the surface will be an N^3 order function. The atomic coordinates of the two molecules are projected onto a grid of $N \times N \times N$ points, allowing each molecule to be described by a discrete function. As a measure of the intermolecular contact, the correlation between the discrete representations of the two macromolecules is calculated. A good contact is represented by a high value of the correlation function. The penetration of two molecules is penalized with a negative-value contribution to the correlation function. In its most straightforward form, this calculation scales as $N^3 \times N^3$. To make the calculation of the correlation function computationally

feasible, the projected representations of both the protein and the ligand are discrete Fourier transformed. As a result, an N^6 order sum is reduced to $N^3 \ln(N^3)$ order. A total of 2000 dimer decoy structures were generated. We used only the coordinates of the heavy atoms. With the position of one peptide fixed, all positions and orientations of the second peptide were searched. The result of the dimer decoy set will not be influenced by which monomer is held fixed and which is moved around the other to match their surfaces. Even with both monomers mobile during the search, the decoy set will have the same composition. A grid step of 1.7 Å, and a step for the search through the rotational coordinates of 10 degrees, were used. The resulting structures were further minimized using the program CHARMM³⁹ version c29b1 with the PARAM22⁴⁰ all-atom potential function.

Desolvation energy screening

An extension of the residue-residue potential contact method proposed by Miyazawa & Jernigan⁴¹ was used to calculate the contribution of the desolvation energy to the binding free energy. The resolution of the calculation of the desolvation energy was increased by estimating the work necessary to transfer different types of atoms from water to the non-polar protein interior.²⁷ The atomic contact energy (ACE) involves the calculation of the number of different atom-atom pair types at the dimer interface using a 6.0 Å cutoff. Only the heavy atoms are considered and they are grouped in 18 classes.²⁷ The backbone, C $^\beta$ and C $^\gamma$ atoms were grouped based on energetic and chemical similarities, while the remaining atoms were grouped according to their chemical properties and cooperative interactions.²⁷ The desolvation energy is written as:

$$\Delta E_{\text{desolv}} = \sum_{i=1}^{18} \sum_{j=1}^{18} e_{ij} n_{ij} \quad (4)$$

where e_{ij} is the work necessary to bring into contact two atoms i and j which belong to different molecules; n_{ij} is the number of the i - j contacts at the intermolecular interface within a r_{cutoff} ($=6.0$ Å) distance. This simple estimation was used to discriminate between well-formed and weakly associated dimer structures.

Molecular dynamics

The molecular dynamics simulations were carried out using the program CHARMM³⁹ version c29b1 with the PARAM22⁴⁰ all-atom force field. The solvent was treated explicitly using the TIP3P three-site rigid model for water molecules.⁴² For the initial coordinates of the unstructured monomers, the NMR structure of A β_{10-35} -NH₂ (410 atoms) was used.²² The protonation state of the titratable amino acid residues was fixed to the expected values at neutral pH in all simulations. The dimer was centered in a truncated octahedron cell that was carved from a larger pre-equilibrated cell of pure water. The size of the primary cell was set according to the minimum-image convention and periodic boundary conditions. The potential energy of the system was minimized until the RMS gradient of the potential energy was less than 0.1 kcal/mol/Å while the dimer atoms were fixed in their positions. To remove steric clashes between atoms, the steepest descent energy minimization algorithm was used for an initial 200 minimization steps; to achieve a desired maximum potential gradient, the adopted basis

Newton–Raphson algorithm was applied for the remainder of the minimization.

The system was linearly heated to 300 K for 120 ps followed by an equilibration phase involving two steps. The system was equilibrated for 80 ps using NVE molecular dynamics with a leapfrog integrator, followed by an additional 70 ps of NPT molecular dynamics. The pressure was restrained to 1 atm using a variant of the extended system method, the Langevin piston algorithm.⁴³ The temperature was restrained to 300 K using the Nosé–Hoover thermostat.⁴⁴ During the heating and the NVE equilibration phases, the velocities were assigned according to a Gaussian distribution. In order to prevent any conformational change of the peptide during the heating and equilibration phases, the dimer atoms were harmonically restrained. To assure a gradual equilibration of the water surrounding the dimer, the restraints were gradually reduced to zero. The center of mass of the dimer was constrained to the center-of-mass of the box of water using the MMFP utility implemented in CHARMM. The electrostatic interactions were calculated with no truncation, using the particle mesh Ewald summation algorithm⁴⁵ with a FFT grid point spacing of 0.95 Å, and a fifth-degree B-spline interpolation. The width of the Gaussian distribution in real-space was 0.32 Å⁻¹. The real-space electrostatic and van der Waals interactions were smoothly shifted to zero at 10 Å, using an atom-based cutoff. The list of the non-bonded interactions was truncated at 12 Å. The lengths of the bonds containing hydrogen atoms were fixed with the SHAKE algorithm⁴⁶ and the equation of motion was iterated using a time step of 2 fs in the leapfrog integrator.

The umbrella sampling method²⁶ was used to determine the profile of the PMF²⁵ along a coordinate ξ . This method implies the constraint of the chosen coordinate in narrow, successive windows i centered on ξ_i^0 , in order to improve the statistical sampling. In this case, the distance between the centers-of-mass (DCOMs) of the two monomers was adopted as the coordinate ξ . A harmonic potential was used to bias the dynamics of the system:

$$U_i(\xi) = \frac{1}{2}k(\xi - \xi_i^0)^2 = \frac{1}{2}k(\xi - \xi_{\text{cont}} - \delta_i^0)^2 \quad (5)$$

where ξ_{cont} is the DCOMs between the two monomers when they are in contact, and δ_i^0 is the surface separation along the coordinate ξ , corresponding to different windows. The time evolution of the DCOMs was saved every 20 fs while the coordinates of the system were saved every 0.2 ps. A force constant of 20 kcal/mol was used for each window. The UMBRELLA facility⁴⁷ of CHARMM was used to bias the distance between the centers-of-mass. The constrained dynamics was computed in 19 windows centered on $\delta_i^0 = 0.0, 0.5, 1.0, \dots, 9.0$ Å. The unphysical contribution of the constraining potential on the overall evolution of the system gives the PMF corresponding to each window:

$$W_i = -kT \ln(\rho_i(\xi)) - U_i(\xi) + C_i \quad (6)$$

where $\rho_i(\xi)$ is the density probability of DCOMs in the i th window, and C_i is a constant that was computed using the weighted histogram analysis method (WHAM).^{48,49}

Secondary structure analysis

The random coil, α -helix, and β -strand structures were determined according with the specific values of the dihedral ϕ and ψ angles. We used the “broad” definition of Munoz & Serrano⁵⁰ for the secondary structure motifs. They assume that the α -helix domain is included in a

polygon defined by the ϕ - ψ coordinates $\{(-90, 0), (-90, -54), (-72, -54), (-72, -72), (-36, -72), (-36, -18), (-54, -18), (-54, 0)\}$, while the β -strand is given by the polygon $\{(-180, 180), (-180, 126), (-162, 126), (-162, 108), (-144, 108), (-144, 90), (-50, 90), (-50, 180)\}$.

Acknowledgements

J.E.S. & D.T. gratefully acknowledge the National Institutes of Health (R01-NS041356) for the generous support. The authors thank Dr Alan Grossfield for making accessible his WHAM code used in the computation of the PMF.

References

- Glenner, G. G. & Wong, C. W. (1984). Alzheimer's disease: initial report of the purification and characterization of a novel cerebrovascular amyloid protein. *Biochem. Biophys. Res. Commun.* **120**, 885–890.
- Masters, C. L., Simms, G., Weinman, N. A., Multhaup, G., McDonald, B. L. & Beyreuther, K. (1985). Amyloid plaque core protein in Alzheimer disease and Down syndrome. *Proc. Natl Acad. Sci. USA*, **82**, 4245–4249.
- Selkoe, D. J. (1991). Alzheimer's disease: a central role for amyloid. *J. Neuropath.* **53**, 438–447.
- Roher, A. E., Ball, M. J., Bhave, S. V. & Wakade, A. R. (1991). β -Amyloid from Alzheimer disease brains inhibits sprouting and survival of sympathetic neurons. *Biochem. Biophys. Res. Commun.* **174**, 572–579.
- Games, D., Adams, D., Alessrini, R., Barbour, R., Bathelette, P., Blackwell, C. *et al.* (1995). Alzheimer-type neuropathology in transgenic mice overexpressing V717F β -amyloid precursor protein. *Nature*, **373**, 523–527.
- LaFerla, F. M., Tinkle, B. T., Bieberich, C. J., Hudenschild, C. C. & Jay, G. (1995). The Alzheimer A β peptide induces neurodegeneration and apoptotic cell death in transgenic mice. *Nature Genet.* **9**, 21–29.
- Hardy, J. & Selkoe, D. J. (2002). The amyloid hypothesis of Alzheimer's disease: progress and problems on the road to therapeutics. *Science*, **297**, 353–356.
- Lambert, M. P., Barlow, A. K., Chromy, B. A., Edwards, C., Freed, R., Liosatos, M. *et al.* (1998). Diffusible, nonfibrillar ligands derived from A β_{1-42} are potent central nervous system neurotoxins. *Proc. Natl Acad. Sci. USA*, **95**, 6448–6453.
- Walsh, D. M., Hartley, D. M., Kusumoto, Y., Fezoui, Y., Condron, M. M., Lomakin, A. *et al.* (1999). Amyloid β -protein fibrillogenesis. Structure and biological activity of protofibrillar intermediates. *J. Biol. Chem.* **274**, 25945–25952.
- Harper, J. D. & Lansbury, P. T. (1997). Models of amyloid seeding in Alzheimer's disease and scrapie: mechanistic truths and physiological consequences of the time-dependent solubility of amyloid proteins. *Annu. Rev. Biochem.* **66**, 385–407.
- Bitan, G., Kirkitadze, M. D., Lomakin, A., Vollers, S. S., Benedek, G. B. & Teplow, D. B. (2003). Amyloid β -protein (A β) assembly: A β 40 and A β 42 oligomerize through distinct pathways. *Proc. Natl Acad. Sci. USA*, **100**, 330–335.
- Massi, F., Klimov, D., Thirumalai, D. & Straub, J. E. (2002). Charge states rather than propensity for

- β -structure determine enhanced fibrillogenesis in wild-type Alzheimer's β -amyloid peptide compared to E22Q Dutch mutant. *Protein Sci.* **11**, 1639–1647.
13. Bitan, G., Tarus, B., Vollers, S. S., Lashuel, H. A., Condrón, M. M., Straub, J. E. & Teplow, D. B. (2003). A molecular switch in amyloid assembly: Met35 and amyloid β -protein oligomerization. *J. Am. Chem. Soc.* **125**, 15359–15365.
 14. Jarrett, J. T., Berger, E. P. & Lansbury, P. T., Jr (1993). The carboxy terminus of the β amyloid protein is critical for the seeding of amyloid formation: Implications for the pathogenesis of Alzheimer's disease. *Biochemistry*, **32**, 4693–4697.
 15. Jarrett, J. T., Berger, E. P. & Lansbury, P. T., Jr (1993). The C-terminus of the beta protein is critical in amyloidogenesis. *Ann. N.Y. Acad. Sci.* **695**, 144–148.
 16. Thirumalai, D., Klimov, D. K. & Dima, R. I. (2003). Emerging ideas on the molecular basis of protein and peptide aggregation. *Curr. Opin. Struct. Biol.* **13**, 146–159.
 17. Burkoth, T. S., Benzinger, T., Urban, V., Morgan, D. M., Gregory, D. M., Thiyagarajan, P. *et al.* (2000). Structure of the β -amyloid(10-35) fibril. *J. Am. Chem. Soc.* **122**, 7883–7889.
 18. Antzutkin, O. N., Balbach, J. J., Leapman, R. D., Rizzo, N. W., Reed, J. & Tycko, R. (2000). Multiple quantum solid-state NMR indicates a parallel, not antiparallel, organization of β -sheets in Alzheimer's β -amyloid fibrils. *Proc. Natl Acad. Sci. USA*, **97**, 13045–13050.
 19. Petkova, A. T., Ishii, Y., Balbach, J. J., Antzutkin, O. N., Leapman, R. D., Delaglio, F. & Tycko, R. (2002). A structural model for Alzheimer's β -amyloid fibrils based on experimental constraints from solid state NMR. *Proc. Natl Acad. Sci. USA*, **99**, 16742–16747.
 20. Kirkitadze, M. D., Condrón, M. M. & Teplow, D. B. (2001). Identification and characterization of key kinetic intermediates in amyloid β -protein fibrillogenesis. *J. Mol. Biol.* **312**, 1103–1119.
 21. Klimov, D. K. & Thirumalai, D. (2003). Dissecting the assembly of A β 16-22 amyloid peptides into antiparallel β -sheets. *Structure*, **11**, 295–307.
 22. Zhang, S., Iwata, K., Lachenmann, M. J., Peng, J. W., Li, S., Stimson, E. R. *et al.* (2000). The Alzheimer's peptide A β adopts a collapsed coil structure in water. *J. Struct. Biol.* **130**, 130–141.
 23. Esler, W. P., Felix, A. M., Stimson, E. R., Lachenmann, M. J., Ghilardi, J. R., Lu, Y. A. *et al.* (2000). Activation barriers to structural transition determine deposition rates of Alzheimer's disease A β amyloid. *J. Struct. Biol.* **130**, 174–183.
 24. Katchalski-Katzir, E., Shariv, I., Eisenstein, M., Friesem, A. A., Aflalo, C. & Vakser, I. A. (1992). Molecular surface recognition: determination of geometric fit between proteins and their ligands by correlation techniques. *Proc. Natl Acad. Sci. USA*, **89**, 2195–2199.
 25. Kirkwood, J. G. (1935). Statistical mechanics of fluid mixtures. *J. Chem. Phys.* **3**, 300–313.
 26. Torrie, G. M. & Valleau, J. P. (1977). Nonphysical sampling distribution in Monte Carlo free-energy estimation: umbrella sampling. *J. Comp. Phys.* **23**, 187–199.
 27. Zhang, C., Vasmatzis, G., Cornette, J. L. & DeLisi, C. (1997). Determination of atomic desolvation energies from the structures of crystallized proteins. *J. Mol. Biol.* **267**, 707–726.
 28. Massi, F., Peng, J. W., Lee, J. P. & Straub, J. E. (2001). Simulation study of the structure and dynamics of the Alzheimer's amyloid peptide congener in solution. *Biophys. J.* **80**, 31–44.
 29. Massi, F. & Straub, J. E. (2001). Energy landscape theory for Alzheimer's amyloid β -peptide fibril elongation. *Proteins: Struct. Funct. Genet.* **42**, 217–229.
 30. Chiti, F., Stefani, M., Taddei, N., Ramponi, G. & Dobson, C. M. (2003). Rationalization of the effects of mutations on peptide and protein aggregation rates. *Nature*, **424**, 805–808.
 31. Chen, R., Li, L. & Weng, Z. (2003). ZDOCK: an initial-stage protein-docking algorithm. *Proteins: Struct. Funct. Genet.* **52**, 80–87.
 32. Chen, R. & Weng, Z. (2002). Docking unbound proteins using shape complementarity, desolvation, and electrostatics. *Proteins: Struct. Funct. Genet.* **47**, 281–294.
 33. Miravalle, L., Tokuda, T., Chiarle, R., Giaccone, G., Bugiani, O. & Tagliavini, F. (2000). Substitutions at codon 22 of Alzheimer's A β peptide induce diverse conformational changes and apoptotic effects in human cerebral endothelial cells. *J. Biol. Chem.* **275**, 27110–27116.
 34. Massi, F. & Straub, J. E. (2001). Probing the origins of increased activity of the E22Q "Dutch" mutant Alzheimer's β -amyloid peptide. *Biophys. J.* **81**, 697–709.
 35. Lee, B. & Richards, F. M. (1971). Interpretation of protein structures: estimation of static accessibility. *J. Mol. Biol.* **55**, 379–400.
 36. Im, W., Beglov, D. & Roux, B. (1998). Continuum solvation model: computation of electrostatic forces from numerical solutions to the Poisson-Boltzmann equation. *Comput. Phys. Commun.* **111**, 59–75.
 37. Zhang, S., Casey, N. & Lee, J. P. (1998). Residual structure in the Alzheimer's disease peptide: probing the origin of a central hydrophobic cluster. *Fold. Des.* **3**, 414–422.
 38. Widom, B., Bhimalapuram, P. & Koga, K. (2003). The hydrophobic effect. *Phys. Chem. Chem. Phys.* **5**, 3085–3093.
 39. Brooks, B. R., Bruccoleri, R., Olafson, B., States, D., Swaminathan, S. & Karplus, M. (1983). CHARMM: a program for macromolecular energy, minimization and dynamics calculations. *J. Comp. Phys.* **4**, 187–217.
 40. MacKerell, A. D., Jr, Bashford, D., Bellott, M., Dunbrack, R. L., Jr, Evanseck, J. D., Field, M. J. *et al.* (1998). All-atom empirical potential for molecular modeling and dynamics studies of proteins. *J. Phys. Chem. B*, **102**, 3586–3616.
 41. Miyazawa, S. & Jernigan, R. L. (1985). Estimation of effective interresidue contact energies from protein crystal structures: quasi-chemical approximation. *Macromolecules*, **18**, 534–552.
 42. Jorgensen, W. L., Chandrasekhar, J., Madura, J. D., Impey, R. W. & Klein, M. L. (1983). Comparison of simple potential functions for simulating liquid water. *J. Chem. Phys.* **79**, 926–935.
 43. Feller, S. E., Zhang, Y., Pastor, R. W. & Brooks, B. R. (1995). Constant pressure molecular dynamics simulation: the Langevin piston method. *J. Chem. Phys.* **103**, 4613–4621.
 44. Hoover, W. G. (1985). Canonical dynamics: equilibrium phase-space distributions. *Phys. Rev. A*, **31**, 1695–1697.
 45. Darden, T., York, D. & Pedersen, L. (1993). Particle mesh Ewald: an $N \log(N)$ method for Ewald sums in large systems. *J. Chem. Phys.* **98**, 10089–10092.
 46. Ryckaert, J. P., Ciccotti, G. & Berendsen, H. J. C. (1977).

- Numerical-integration of Cartesian equations of motion of a system with constraints: molecular dynamics of *n*-alkanes. *J. Comp. Phys.* **23**, 327–341.
47. Kottalam, J. & Case, D. A. (1988). Dynamics of ligand escape from the heme pocket of myoglobin. *J. Am. Chem. Soc.* **110**, 7690–7697.
48. Kumar, S., Bouzida, D., Swendsen, R. H., Kollman, P. A. & Rosenberg, J. M. (1992). The weighted histogram analysis method for free-energy calculations on biomolecules. I. The method. *J. Comp. Chem.* **13**, 1011–1021.
49. Roux, B. (1995). The calculation of the potential of mean force using computer simulations. *Comput. Phys. Commun.* **91**, 275–282.
50. Munoz, V. & Serrano, L. (1994). Intrinsic secondary structure propensities of the amino acids, using statistical ϕ - ψ matrices: comparison with experimental scales. *Proteins: Struct. Funct. Genet.* **20**, 301–311.

Edited by P. T. Lansbury Jr

(Received 26 July 2004; received in revised form 22 October 2004; accepted 8 November 2004)